included ($n = 63$), the first two P values are 0.002 ($\chi^2 = 9.654$) and 0.022 ($\chi^2 = 5.276$), respectively, and the third $P = 0.587$ ($\chi^2 = 0.295$). The logistic procedure of SAS software was used for all computations.
20. None of the 65 such lizards exceeded 34 mm in snout-vent length, and only one other was larger than 31 mm. Maximum snout-vent length in *A. sagrei* in this region of the Bahamas is 57 mm for males and 44 mm for females.
21. For November 1999, score chi-squares for altitude and log area both give $P < 0.0001$ ($\chi^2 = 39.359$ and 28.758, respectively). Once altitude is added, score chi-square for log area gives $P = 0.328$ ($\chi^2 = 0.959$). For April 2000, score chi-squares for altitude and log area both give $P < 0.0001$ ($\chi^2 = 22.221$ and 21.259, respectively). Once altitude is added, score chi-square for log area gives $P = 0.151$ ($\chi^2 = 2.067$). For November 2000, score chi-squares for altitude and log area both give $P < 0.0001$ ($\chi^2 = 16.107$ and 22.856, respectively). Once log area is added, score chi-square for altitude gives $P = 0.135$ ($\chi^2 = 2.230$). For April 2001, score chi-squares for altitude and log area give $P = 0.0002$ ($\chi^2 = 13.632$) and $P < 0.0001$ ($\chi^2 = 19.195$), respectively. Once log area is added, score chi-square for altitude gives $P = 0.163$ ($\chi^2 = 1.948$). Introduction islands are included in all analyses.
22. J. M. Diamond, R. M. May, *Science* **197**, 266 (1977).
23. P. Licht, G. C. Gorman, *Univ. Calif. Publ. Zool.* **95**, 1 (1970).
24. J. H. Connell, *Science* **199**, 1302 (1978).
25. W. P. Sousa, *Annu. Rev. Ecol. Syst.* **15**, 353 (1984).
26. S. T. A. Pickett, P. S. White, *The Ecology of Natural Disturbance and Patch Dynamics* (Academic Press, New York, 1985).
27. J. Vandermeer, I. G. de la Cerda, D. Boucher, I. Perfecto, J. Ruiz, *Science* **290**, 788 (2000).
28. I. Thornton, *Krakatoa* (Harvard Univ. Press, Cambridge, MA, 1996).
29. D. R. Townes, C. H. Daugherty, I. A. E. Atkinson, *Ecological Restoration of New Zealand Islands* (Department of Conservation, Wellington, New Zealand, 1990).
30. T. W. Schoener, *Am. Nat.* **131**, 847 (1988).
31. _____, A. Schoener, *Nature* **302**, 332 (1983).
32. T. W. Schoener, D. A. Spiller, *Am. Nat.* **153**, 347 (1999).
33. We thank NSF for support.

16 July 2001; accepted 20 September 2001

Role of Erv29p in Collecting Soluble Secretory Proteins into ER-Derived Transport Vesicles

William J. Belden and Charles Barlowe*

Proteins are transported from the endoplasmic reticulum (ER) in vesicles formed by coat protein complex II (COPII). Soluble secretory proteins are thought to leave the ER in these vesicles by "bulk flow" or through recognition by hypothetical shuttling receptors. We found that Erv29p, a conserved transmembrane protein, was directly required for packaging glycosylated pro-α-factor (gpαf) into COPII vesicles in *Saccharomyces cerevisiae*. Further, an Erv29p-gpαf complex was isolated from ER-derived transport vesicles. In vivo, export of gpαf from the ER was saturable and depended on the expression level of Erv29p. These results indicate that membrane receptors can link soluble cargo proteins to the COPII coat.

In eukaryotic cells, secretory proteins are packaged into COPII-coated vesicles at the ER for transport through the early secretory pathway. The mechanisms by which secretory proteins are segregated away from ER resident proteins during vesicle formation are still a matter of debate (*1*). Certain portions of integral membrane cargo appear to bind directly to subunits of the COPII coat (*2, 3*), allowing for their concentration into ER-derived vesicles (*4, 5*). It is less clear how soluble secretory cargos are exported from the ER, and evidence supporting bulk flow (*5*) and receptor-mediated export mechanisms (*2, 6*) exists. One difficulty with the receptor model has been the failure to identify integral membrane proteins that could fulfill this function.

In *S. cerevisiae*, COPII-coated vesicle formation has been reconstituted in cell-free reactions using ER membranes and purified COPII components: Sar1p, Sec23p complex, and Sec13p complex (*7*). COPII vesicles have been isolated and several of the abundant integral membrane constituents have been characterized in an effort to identify proteins involved in sorting during vesicle formation (*8*). One such ER-vesicle protein of 29 kD (hence Erv29p) is conserved across species (*9*), is selectively packaged into COPII vesicles (*8*), and contains multiple membrane-spanning domains with a terminal dilysine sorting signal (*10*).

Haploid *erv29Δ* strains are viable and display no observable growth defects (*8, 10*). To test whether *ERV29* deletion influenced protein transport between the ER and Golgi, we performed a reconstituted cell-free assay that measures transport of [^{35}S]gpαf to the Golgi complex (*11*). Surprisingly, no transport of gpαf was detected in membranes lacking Erv29p, although translocation of [^{35}S]prepαf into ER membranes was unaffected. Specifically, the defect in gpαf transport occurred at the COPII-dependent budding step. Budding of gpαf in wild-type membranes was efficient (33% of total), whereas only minor amounts (4% of total) were budded from *erv29Δ* membranes (Fig. 1A). To distinguish whether this result was due to a general decrease in COPII budding or a fail-

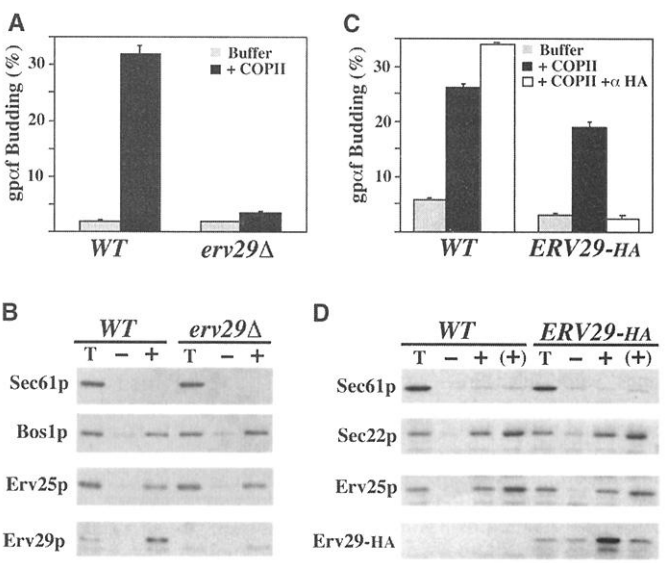

Fig. 1. Erv29p is required for gpαf packaging into COPII vesicles. Reconstituted COPII budding reactions from ER membranes isolated from FY834 (wild type, WT) and CBY966 (*erv29Δ*) are shown (*21*). (**A**) [^{35}S]gpαf budding reactions contained membranes incubated with or without purified COPII proteins (*7*). The percent budding represents the amount of [^{35}S]gpαf released in freely diffusible vesicles divided by the total amount of [^{35}S]gpαf contained in reactions. (**B**) Total membranes and budded vesicles, generated as in (A), were collected by centrifugation, resolved on polyacrylamide gels, and immunoblotted for the indicated proteins (*22*). Lanes labeled T represent one-tenth of the total; minus lanes show vesicles formed in the absence of COPII components; plus lanes show vesicles produced in the presence of COPII proteins. (**C** and **D**) As in (A) and (B), respectively, except that membranes from FY834 (WT) and CBY1160 (ERV29-HA) were used. HA mAb (0.07 mg/ml) was added to COPII budding reactions and is indicated by a bracketed plus sign (+) in (D).

Department of Biochemistry, Dartmouth Medical School, Hanover, NH 03755, USA.

*To whom correspondence should be addressed. E-mail: barlowe@dartmouth.edu

ure to package gpαf into COPII vesicles, we monitored budding of other integral membrane proteins contained on COPII vesicles. Bos1p, an ER/Golgi SNARE (soluble *N*-ethylmaleimide–sensitive factor attachment protein receptor), and Erv25p, a member of the p24 family, were budded with equal efficiency from both wild-type and *erv29Δ* membranes in the presence of COPII proteins (Fig. 1B). Sec61p, an ER resident protein, served as a negative control and indicated selectivity in the budding reaction. Thus, in the absence of Erv29p, COPII vesicles formed normally, but gpαf was not packaged into these vesicles.

To determine whether Erv29p was directly involved in gpαf export, we analyzed COPII vesicle formation and gpαf packaging in wild-type membranes after inhibition of Erv29p function in vitro. We used a hemagglutinin (HA)–tagged version of Erv29p that places three sequential HA epitopes into the NH_2-terminal domain of Erv29p (*10*). Membranes with Erv29-HA as the sole source of Erv29p displayed sensitivity to monoclonal antibody to HA (HA mAb) when gpαf budding was measured (Fig. 1C), whereas strains expressing endogenous Erv29p were insensitive. Furthermore, the packaging of Erv29-HA into COPII vesicles was inhibited when HA mAb was added (Fig. 1D). Presumably, antibody binding to this HA epitope sterically hinders access of coat subunits to Erv29p. The budding efficiencies of other vesicle proteins were not decreased when Erv29-HA function was neutralized; this result indicates that Erv29p function is specifically and directly required for packaging of gpαf into COPII vesicles.

If Erv29p acts in packaging of gpαf into COPII-coated vesicles, *erv29Δ* cells should exhibit a reduced rate of gpαf transport in pulse-chase analyses. In wild-type strains, pαf acquires N-linked core oligosaccharide in the ER, generating the 29-kD gpαf form. Transport through the Golgi complex produces a heterogeneously glycosylated species that is cleaved to generate secreted pheromone (*12*). The ER form of gpαf was exported rapidly in the wild type; however, gpαf accumulated in *erv29Δ* cells, and after a 20-min chase only 45% had been transported from the ER (Fig. 2A). The *sec12-4* temperature-sensitive mutant blocked all export from the ER and demonstrated the characteristic accumulation of secretory proteins in the ER.

Additional secretory proteins were monitored in this pulse-chase experiment. Transport of carboxypeptidase Y (CPY) from the ER was also delayed in *erv29Δ* cells (Fig. 2B). The ER form of CPY (p1) migrates as a 67-kD species that is modified in the Golgi complex to generate the 69-kD p2 form and is then cleaved to the 61-kD mature form upon delivery to the vacuole (*13*). In *erv29Δ* cells, 40% of the CPY remained as the p1 form after a 20-min chase, whereas most of the CPY was fully matured after a 10-min chase in wild-type cells. This is consistent with a reported delay in transport of CPY and proteinase A in *erv29Δ* strains (*10*). This transport defect was specific for a subset of secretory proteins because the GPI-anchored protein Gas1p (Fig. 2C), the soluble secreted protein invertase (Fig. 2D), and vacuolar targeted alkaline phosphatase (*10*) appeared to mature at wild-type rates in *erv29Δ* strains.

In subcellular fractionation experiments, we observed that Erv29p was equally distributed between ER and Golgi membranes (*14*). If Erv29p cycles as a cargo receptor for gpαf, ER export should be saturable and the expression level of Erv29p should influence the export capacity for these secretory proteins.

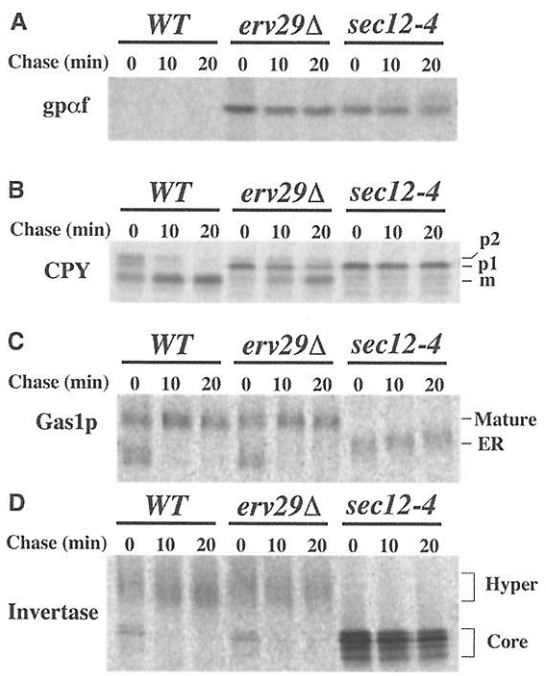

Fig. 2. Cells lacking Erv29p accumulate ER forms of gpαf and CPY, but not Gas1p or invertase. Cell extracts were prepared from FY834 (WT), CBY966 (*erv29Δ*), and RSY263 (*sec12-4*) after a 10-min pulse with ^{35}S-labeled amino acids and chased for the indicated times (*8*). (**A**) gpαf, (**B**) CPY, and (**C**) Gas1p were immunoprecipitated from a common extract and resolved on 10% polyacrylamide gels. (**D**) Invertase pulse-chase analyses were performed with derepressed cells. Proteins were visualized and transport rates quantified using a PhosphorImager (*20*).

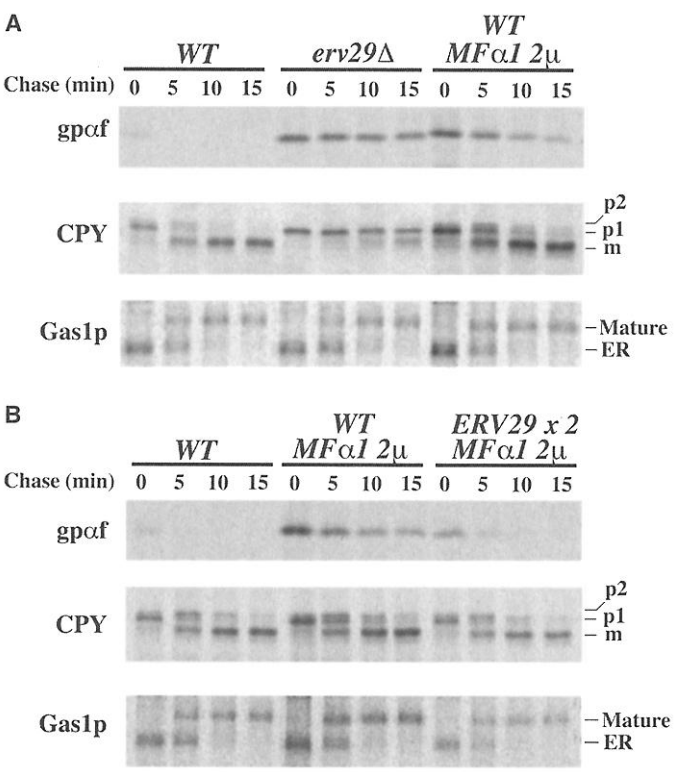

Fig. 3. Expression level of Erv29p influences the transport kinetics of gpαf. (**A**) Cells were pulsed for 5 min with ^{35}S-labeled amino acids, then chased for the indicated times. Proteins were immunoprecipitated from extracts prepared from FY834 (WT), CBY966 (*erv29Δ*), and CBY1161 (WT, *MFα1-2μ*), a strain that overproduces gpαf. (**B**) As in (A), with CBY1162 (*MFα1-2μ*, *ERV29* × *2*), a strain that overproduces gpαf and contains two chromosomal copies of *ERV29*, included. Proteins were visualized and transport rates quantified using a PhosphorImager (*20*).

To test this idea, we overexpressed gpαF (encoded by the *MFα1* gene) and monitored the kinetics of ER export in pulse-chase experiments (Fig. 3A). Overexpression of *MFα1* resulted in a delay by a factor of 4 or more in the transport kinetics of gpαf from the ER. We also detected a modest decrease (factor of 1.3) in the transport rate of p1 CPY under this condition. In contrast, the transport rates of Gas1p and alkaline phosphatase were unaffected by *MFα1* overexpression. Erv29p was limiting under these conditions, because cells with an additional copy of *ERV29* expressed twice the level of Erv29p (*14*) and accelerated the transport kinetics of overproduced gpαf by a factor of 2 (Fig. 3B). These results indicate that transport of gpαf from the ER was saturable, and that increased expression of Erv29p partially alleviated this accumulation. A restoration of CPY transport rate was also observed in this strain (Fig. 3B).

The above results suggested that Erv29p binds gpαf in the ER and forms a receptor-cargo complex for capture into COPII-coated vesicles. To look for such a complex, we immunoprecipitated Erv29p after treating ER membranes containing [^{35}S]gpαf with the thiol-cleavable crosslinker dithiobis(succinimidyl propionate) (DSP). Using antiserum to Erv29p, we coimmunoprecipitated [^{35}S]gpαf with Erv29p in a crosslinker- and Erv29p-dependent manner (Fig. 4A). As an independent method, we also immunoprecipitated [^{35}S]gpαf in complex with Erv29-HA using HA mAb in a reaction that depended on crosslinker (Fig. 4A) and on the presence of HA-tagged Erv29p (*14*). In wild-type microsomes, the recovery of [^{35}S]gpαf in complex with Erv29p was ~0.5% of total; however, only 2% of the total Erv29p could be immunoprecipitated under these conditions. Recovery of [^{35}S]gpαf linked to Erv29-HA was improved (~1% of total) using HA mAb compared with the Erv29p polyclonal antibody, although addition of crosslinker reduced the efficiency of Erv29-HA immunoprecipitation (Fig. 4A). Isolation of the cross-linked Erv29p-gpαf complex appeared specific because no Kar2p (mammalian BiP homolog) was detected in these immunoprecipitations.

To further characterize the composition of the Erv29-gpαf complex, we performed cross-linking experiments with a noncleavable agent, disuccinimidyl glutarate (DSG). COPII vesicles containing [^{35}S]gpαf were generated from wild-type and Erv29-HA microsomes and treated with DSG, and Erv29-[^{35}S]gpαf complexes were isolated by immunoprecipitation with antiserum to Erv29p or with HA mAb (Fig. 4B). Immunoprecipitated proteins were resolved on polyacrylamide gels and distinct Erv29-[^{35}S]gpαf complexes were observed by autoradiography. In wild-type vesicles, primary cross-linked products of about 56 and 85 kD were detected. In Erv29-HA vesicles, analogous products of 61 and 90 kD were observed, with a ~5-kD increase in mass due to the presence of the 3×HA tag. The appearance of a 56-kD radiolabeled species in wild-type vesicles (which is the approximate mass of an Erv29p-[^{35}S]gpαf complex) and a corresponding ~5-kD shift observed in the Erv29-HA vesicles indicated that Erv29p and [^{35}S]gpαf were in direct contact. This finding is in accord with reports proposing that a 27-kD integral membrane protein binds [^{35}S]gpαf specifically in COPII vesicles (*2, 15*). The molecular identity of this vesicle protein appears to be Erv29p. The additional higher molecular weight species in these immunoprecipitates (85 kD in the wild type and 90 kD in Erv29-HA) suggests that a gpαf dimer bound to Erv29p or that Erv29p functioned as a dimer. The major cross-linked product of ~58 kD detected in samples before immunoprecipitation probably represents a gpαf dimer, as previously observed (*2*).

We propose that Erv29p binds to fully folded gpαf and probably to other soluble secretory cargo in the ER, after which Erv29p-cargo complexes are packaged into COPII vesicles for transport to the Golgi complex. Upon delivery to the Golgi, Erv29p-cargo complexes dissociate and empty receptors are recruited into ER-directed COPI vesicles through a dilysine motif present on Erv29p. Similar mechanisms have been proposed for the Emp24 complex (*6*) and ERGIC53 (*16*), integral membrane proteins that also cycle between ER and Golgi compartments. As in these examples, Erv29p has homologs in all higher eukaryotes with sequenced genomes, suggesting a conserved function. In light of recent findings linking ERGIC53 to secretion of blood-clotting factors and to some forms of hemophilia (*17*), it may be informative to investigate mammalian Erv29p. Furthermore, *ERV29* and other conserved genes involved in transport between the ER and Golgi are up-regulated by the unfolded protein response (*18*) and are required for efficient degradation of soluble misfolded substrates (*10*). This induction may serve to clear the ER of soluble misfolded proteins when ER-associated degradation becomes saturated (*10, 18*), although it remains to be determined whether Erv29p acts directly in ER quality control.

Forward transport from the ER is coordi-

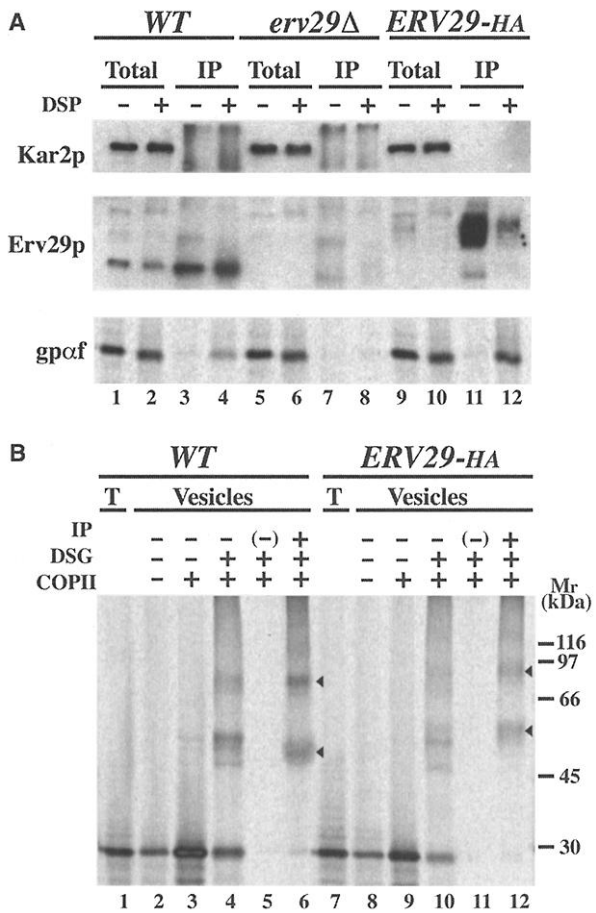

Fig. 4. Isolation and characterization of Erv29p-gpαf complexes. (**A**) Microsomes (0.2 mg) isolated from FY834 (WT), CBY966 (*erv29*Δ), and CBY1160 (*ERV29-HA*) that contained translocated [^{35}S]gpαf were treated with (+) and without (–) DSP (0.5 mM), solubilized in 0.5% SDS, and immunoprecipitated with antiserum to Erv29p (lanes 3, 4, 7, and 8) or HA mAb (lanes 11 and 12) as described (*23*). Immunoprecipitates were reduced and resolved on polyacrylamide gels. Total lanes represent 1% of initial extracts. [^{35}S]gpαf was detected by PhosphorImager analysis and other proteins detected by immunoblot. (**B**) Microsomes (0.35 mg) from FY834 (WT) or CBY1160 (*Erv29-HA*) that contained translocated [^{35}S]gpαf were used to generate vesicles by the addition of purified COPII proteins. Budded vesicles were collected by centrifugation (lanes 3 and 9) or treated with DSG (0.05 mM) and incubated with 0.1 M Na_2CO_3, pH 11.0 (lanes 4 to 6 and 10 to 12) to extract soluble proteins before collecting membranes. For immunoprecipitations, extracted vesicles were solubilized in 0.5% SDS, diluted, and incubated with protein A–Sepharose beads and preimmune serum (lane 5), antiserum to Erv29p (lane 6), beads alone (lane 11), or HA mAb (lane 12). Total lanes (T) represent 5% of starting microsomal extracts. Arrowheads indicate the primary cross-linked products in immunoprecipitates.

nated with a retrograde pathway that recycles vesicle proteins and retrieves escaped ER residents (*19*). Indeed, selective exclusion of secretory cargo from retrograde vesicles may explain the concentration of certain soluble cargo after export from the ER (*5*). Our results indicating Erv29p action as a cargo receptor do not exclude other sorting mechanisms; rather, it now seems probable that multiple mechanisms of retention, retrieval, and selective export operate in concert to achieve organization of the early secretory pathway.

References and Notes

1. G. Warren, I. Mellman, *Cell* **98**, 125 (1999).
2. M. J. Kuehn, J. M. Herrmann, R. Schekman, *Nature* **391**, 187 (1998).
3. S. Springer, R. Schekman, *Science* **281**, 698 (1998).
4. W. E. Balch, J. M. McCaffery, H. Plutner, M. G. Farquhar, *Cell* **76**, 841 (1994).
5. J. A. Martinez-Menarguez, H. J. Geuze, J. W. Slot, J. Klumperman, *Cell* **98**, 81 (1999).
6. M. Muniz, C. Nuoffer, H-P. Hauri, H. Riezman, *J. Cell Biol.* **148**, 925 (2000).
7. C. Barlowe *et al.*, *Cell* **77**, 895 (1994).
8. S. Otte *et al.*, *J. Cell Biol.* **152**, 503 (2001).
9. J. E. Reeves, M. Fried, *Mol. Membr. Biol.* **12**, 201 (1995).
10. S. R. Caldwell, K. J. Hill, A. A. Cooper, *J. Biol. Chem.* **276**, 23296 (2001).
11. C. Barlowe, *J. Cell Biol.* **139**, 1097 (1997).
12. D. Julius, R. Schekman, J. Thorner, *Cell* **36**, 309 (1984).
13. T. Stevens, B. Esmon, R. Schekman, *Cell* **30**, 439 (1982).
14. W. J. Belden, C. Barlowe, unpublished data.
15. S. Y. Bednarek *et al.*, *Cell* **83**, 1183 (1995).
16. C. Appenzeller, H. Andersson, F. Kappeler, H. P. Hauri, *Nature Cell Biol.* **1**, 330 (1999).
17. W. C. Nichols *et al.*, *Cell* **93**, 61 (1998).
18. K. J. Travers *et al.*, *Cell* **101**, 249 (2000).
19. H. R. Pelham, *Curr. Opin. Cell Biol.* **7**, 530 (1995).
20. For data plots of the experiments in Figs. 2 and 3, see *Science* Online (www.sciencemag.org/cgi/content/full/294/5546/1528/DC1).
21. Strain CBY966 (*10*) was transformed with pAC530 (*12*) to generate CBY1160 (*erv29Δ::KAN ERV29-HA*). FY834 (*10*) was transformed with pDA6300 (*Mfα1-LEU2-2μ*) to generate CBY1161. CBY1162 contains *pRS306-ERV29* integrated into the *URA3* locus of CBY1161.
22. Antiserum to Erv29p was raised against a GST-Erv29p fusion protein. A 262–base pair 5′ Apo I fragment from *ERV29* was inserted into pGEX-5x-3, and fusion protein was purified as described by the manufacturer (Amersham Pharmacia). Antiserum was produced in rabbits by Covance Inc. (Denver, PA).
23. Cross-linking reactions (0.05 ml) were performed in buffer 88 [25 mM Hepes (pH 7.5), 150 mM KOAc, 0.25 M sorbitol, and 5 mM MgOAc] for 20 min at 20°C. Reactions were quenched with 10 mM glycine for 5 min at 20°C, solubilized with an equal volume of 1% SDS, and heat-denatured. Where indicated, proteins were immunoprecipitated with antibodies after dilution with 1 ml of IP buffer [15 mM tris-Cl (pH 7.5), 150 mM NaCl, and 1% Triton X-100].

24. We thank A. Cooper for providing the HA-tagged Erv29p construct, R. Gilmore for antiserum to CPY, and R. Schekman for antiserum to αf. Supported by grants from the National Institute of General Medical Sciences and the Pew Scholars Program in the Biomedical Sciences.

9 August 2001; accepted 28 September 2001

Lack of Acrosome Formation in Hrb-Deficient Mice

Ningling Kang-Decker,[1] George T. Mantchev,[1] Subhash C. Juneja,[1] Mark A. McNiven,[2,3] Jan M. A. van Deursen[1]*

The sperm acrosome is essential for sperm-egg fusion and is often defective in men with nonobstructive infertility. Here we report that male mice with a null mutation in Hrb are infertile and display round-headed spermatozoa that lack an acrosome. In wild-type spermatids, Hrb is associated with the cytosolic surface of proacrosomic transport vesicles that fuse to create a single large acrosomic vesicle at step 3 of spermiogenesis. Although proacrosomic vesicles form in spermatids that lack Hrb, the vesicles are unable to fuse, blocking acrosome development at step 2. We conclude that Hrb is required for docking and/or fusion of proacrosomic vesicles during acrosome biogenesis.

The acrosome is a unique membranous organelle that is formed during spermiogenesis through an integrated process of transport vesicle production, trafficking, and fusion (*1*, *2*). In the first period of acrosome biogenesis, the Golgi phase, numerous small proacrosomic vesicles accumulate in the medulla, a cytoplasmic compartment located between the juxta-nuclear Golgi apparatus and the nuclear surface. There, they coalesce into a single spherical acrosomic vesicle that attaches to the nucleus. During the subsequent Cap phase, the acrosomic vesicle expands by means of sustained vesicular membrane transport and fusion. At the onset of sperm elongation, the acrosomic vesicle stops growing in size and starts undergoing a series of highly complex morphological changes that shape the sperm cell. Little is known about the molecular mechanisms that regulate the targeting and fusion of transport vesicles during acrosomic vesicle formation, although the understanding of this process is highly relevant because disturbances of acrosomal development and function perturb the fertilizing capacity of spermatozoa (*3*, *4*).

Here we identify the Asn-Pro-Phe (NPF) motif-containing protein Hrb (also called Rab or hRip) (*5*–*7*) as a component that is essential for acrosome formation. We addressed the physiological role of Hrb through targeted inactivation of the Hrb gene in the mouse (*8*, *9*). $Hrb^{-/-}$ mice were indistinguishable from $Hrb^{+/-}$ and $Hrb^{+/+}$ mice, had a normal life-span, and showed no apparent histological abnormalities in brain, colon, heart, kidney, liver, lung, spleen, or thymus. Western blot analysis confirmed that the mutant Hrb allele was null (*8*, *9*). Despite normal sexual behavior and copulation, $Hrb^{-/-}$ males derived from two independently targeted embryonic stem cell (ES) clones were infertile. By contrast, $Hrb^{-/-}$ females displayed normal fertility. The average testicular weight in 10-week-old $Hrb^{-/-}$ mice [0.079 g ± 0.1 (n = 12 testes)] was not significantly different from that in wild-type mice [0.082 g ± 0.09 (n = 12 testes)]. However, $Hrb^{-/-}$ mice contained on average ~15-fold less spermatozoa in the cauda epididymis than wild-type males (*8*). The spermatozoa from mutant males showed severely reduced motility and several structural abnormalities. The spermatozoa displayed a globic head (Fig. 1A) with a round nucleus and a tail midpiece lacking the mitochondrial sheath (Fig. 1B) (*8*). This sheath is composed of mitochondria that generate adenosine triphosphate (ATP) for movement of the flagellum and is formed in the final steps of normal spermatid elongation (*2*). In vitro fertilization experiments revealed that $Hrb^{-/-}$ spermatozoa were unable to establish sperm-egg attachment and fertilization (Fig. 1C) (*8*).

β-galactosidase staining of the testis of $Hrb^{+/-}$ mice indicted that the Hrb gene was abundantly transcribed during spermiogenesis (*9*). Histological analysis of testis sections showed that seminiferous-tubule diameters in $Hrb^{+/+}$ and $Hrb^{-/-}$ mice were comparable (*9*). The number and distribution of mitotic (spermatogonia) and meiotic (spermatocytes) germ cells in these tubules also appeared to be similar (Fig. 2, A and B) (*8*). The appearance of interstitial cells was also normal. However, the process of transformation of round spermatids into testicular spermatozoa (spermiogenesis) was clearly disrupted in $Hrb^{-/-}$ mutants. Typically, mutant tubules were devoid of elongated spermatids and contained exclusively round-headed spermatids (Fig. 2B) (*9*). Although acrosomes were easily detectable in wild-type round spermatids by light microscopy and by transmission electron microscopy (TEM) (Fig. 2, A and C) (*8*), no acrosome structures were visible in mu-

[1]Department of Pediatrics and Adolescent Medicine, [2]Department of Biochemistry and Molecular Biology, [3]Department of Gastroenterology and Hepatology, Mayo Clinic, 200 First Street SW, Rochester, MN 55905, USA.

*To whom correspondence should be addressed. E-mail: vandeursen.jan@mayo.edu